

MOLECULAR DYNAMICS SIMULATIONS OF M2 CHANNEL IN PHOSPHOLIPID BILAYERS
WITH DIFFERENT THICKNESS



A Thesis Submitted in Partial Fulfillment of the Requirements
for the Degree of Master of Science in Chemistry

Department of Chemistry

FACULTY OF SCIENCE

Chulalongkorn University

Academic Year 2019

Copyright of Chulalongkorn University

การจำลองพลวัตเชิงโมเลกุลของเอ็มทูแซนแนลในฟอสฟอลิพิดไบเลเยอร์ที่มีความหนาต่างกัน



วิทยานิพนธ์นี้เป็นส่วนหนึ่งของการศึกษาตามหลักสูตรปริญญาวิทยาศาสตรมหาบัณฑิต

สาขาวิชาเคมี ภาควิชาเคมี

คณะวิทยาศาสตร์ จุฬาลงกรณ์มหาวิทยาลัย

ปีการศึกษา 2562

ลิขสิทธิ์ของจุฬาลงกรณ์มหาวิทยาลัย

ชาญณรงค์ ครุฑโต : การจำลองพลวัตเชิงโมเลกุลของเอ็มทูแซนแนลในฟอสโฟลิพิดไบเลเยอร์ที่มีความหนาต่างกัน. (MOLECULAR DYNAMICS SIMULATIONS OF M2 CHANNEL IN PHOSPHOLIPID BILAYERS WITH DIFFERENT THICKNESS) อ.ที่ปรึกษาหลัก : ศ. ดร.พรเทพ สมพรพิสุทธิ์

งานวิจัยก่อนหน้า 2 ชิ้นได้แสดงให้เห็นว่าเอ็มทูแซนแนลโปรตีนที่มีบทบาทสำคัญในการจำลองตัวเองของไวรัสฮีนฟลูเอนซาได้มีการว่าตัวที่แตกต่างกันตามความหนาของเยื่อหุ้มฟอสโฟลิพิดศึกษาโดยใช้เทคนิค ไซโตโตเรคสปินเลเบล อีพีอาร์ สเปกโตรสโกปี งานวิจัยชิ้นหนึ่งได้ตีความสารประกอบที่มีอิเล็กตรอนพาราแมกเนติกบนปลายด้านเอ็น ส่วนอีกงานวิจัยหนึ่ง บนปลายด้านซี งานวิจัยทั้งสองชิ้นนี้สนับสนุนซึ่งกันและกันว่ายี่เยื่อหุ้มฟอสโฟลิพิดมีความหนาเท่าใดก่อนทรานส์เมมเบรนก็จะเอียงน้อยลงเท่านั้น คณะผู้ทำงานวิจัยทั้งสองชิ้นได้สรุปว่าการวางตัวของเอ็มทูแซนแนลขึ้นอยู่กับความหนาของเยื่อหุ้มฟอสโฟลิพิด แต่ข้อมูลที่ได้จากเทคนิคนี้ยังมีความกำกวม ค่าสปิน-สปิน คลັปปิงไม่สามารถแยกแยะได้ว่าเกิดจากก่อนของทรานส์เมมเบรนที่อยู่ตรงกันข้ามกันหรืออยู่ถัดจากกัน เนื่องจากรายละเอียดที่แม่นยำในระดับโมเลกุลด้วยเทคนิคนี้ยังมีข้อจำกัดอยู่ การจำลองทางคอมพิวเตอร์จึงมีความสำคัญ คณะผู้วิจัยได้ใช้วิธีพลวัตเชิงโมเลกุลศึกษาการวางตัวของเอ็มทูแซนแนลในเยื่อหุ้มฟอสโฟลิพิดที่มีความหนาแตกต่างกัน โดยจำลองเอ็มทูแซนแนลที่ถูกฝังใน DLPC, DMPC และ POPC ในสภาวะธรรมชาติ (ไม่ได้มีการติดฉลากสปิน) ติดฉลากสปินบนปลายด้านซี และ ติดฉลากสปินบนปลายด้านซีและมีการจำกัดการเคลื่อนไหวของปลายของเอ็มทูแซนแนลที่จะเป็นผลมาจากความหนาของเยื่อหุ้มฟอสโฟลิพิด การวิเคราะห์ผลลัพธ์ของการจำลองทางคอมพิวเตอร์ได้แสดงให้เห็นว่าในสภาวะธรรมชาติ เอ็มทูแซนแนลไม่ได้มีการเปลี่ยนแปลงการวางตัวในการฟอสโฟลิพิดที่มีความหนาแตกต่างกันแต่เกิดจากการรบกวนของสารประกอบที่มีสปินที่ติดฉลากบนเอ็มทูแซนแนล การเอียงตัวของเอ็มทูแซนแนลไม่ได้มีความสัมพันธ์กับความหนาของเยื่อหุ้มฟอสโฟลิพิด และความอิสระของปลายของก่อนโปรตีนของเอ็มทูแซนแนลไม่ได้มีผลต่อการวางตัวของโปรตีน

สาขาวิชา เคมี
ปีการศึกษา 2562

ลายมือชื่อนิสิต
ลายมือชื่อ อ.ที่ปรึกษาหลัก

5971939223 : MAJOR CHEMISTRY

KEYWORD: Influenza A Virus, M2 Channel, Membrane Thickness, MD simulation
 Channarong Khрутto : MOLECULAR DYNAMICS SIMULATIONS OF M2
 CHANNEL IN PHOSPHOLIPID BILAYERS WITH DIFFERENT THICKNESS. Advisor:
 Prof. PORNTHEP SOMPORNPIST, Ph.D.

Two previous studies showed that M2 channel, a viral protein plays important role in replication of influenza virus, had different conformation after phospholipid bilayers thickness by using site-directed spin-label EPR spectroscopy (SDSL/EPR), one study, the M2 was spin-labeled on N-terminal amino acid residues, another one the M2 was spin-labeled on the C-terminal amino acid residues. Both studies supported each another. The more thickness phospholipid bilayer is the higher spin coupling value. It can be concluded that the conformation of M2 channel depends on phospholipid bilayer thickness. Data got from this technique is ambiguous, spin-spin coupling cannot be distinguishable, diagonal distance pairs or lateral distance pairs. Precise detail on molecular were limited, so computer simulation was required. We used molecular dynamic to study. We simulated and performed embed M2 channel in 3 different thickness phospholipids, DLPC, DMPC and POPC in nature condition (none spin-labeling), C-terminal spin-labeling. For confirmation that of the conformation changing was not cause by freedom of terminal ends, the C-terminal spin-labeling with terminals constrained systems were performed. Instead of the thickness of the membrane, trajectories analysis show that conformational changes were caused by perturbation of spin-labeling compound, MTSSL. In addition, distance between subunit of the protein have no relation to the thickness of the membrane and freedom of the terminal end.

Field of Study: Chemistry

Student's Signature

Academic Year: 2019

Advisor's Signature

ACKNOWLEDGEMENTS

This thesis could not be complete, if there are support from all of these person

I would like to deeply and sincerely thank to my advisor, Prof. Dr. Pornthep Sompornpisut, teaching and consulting me all during research proccess

I would like to thank my thesis committee, Assoc. Prof. Dr. Vudhichai Parasuk, Assist. Prof. Dr. Somsak Pianwanit,

The scholarship from the graduate school, Chulalongkorn university to commemorate the 72nd anniversary of his Majesty King Bhumibol Aduadej and the 90th Anniversary Chulalongkorn University Fund (Ratchadaphiseksomphot Endownet Fund) are gratefully acknowledged

Channarong Khrutto



TABLE OF CONTENTS

	Page
.....	iii
ABSTRACT (THAI).....	iii
.....	iv
ABSTRACT (ENGLISH).....	iv
ACKNOWLEDGEMENTS.....	v
TABLE OF CONTENTS.....	vi
LIST OF TABLES.....	viii
LIST OF FIGURES.....	ix
Chapter 1 Introduction.....	1
1.1 Research rationale.....	1
1.2 Literature review.....	7
1.3 scope of this research.....	12
Chapter 2 Theory Background.....	13
2.1 MD Simulation.....	13
2.2.1 Integration algorithm.....	14
2.1.2 Periodic boundary conditions.....	15
2.1.3 Cutoff.....	15
2.1.4 Isobaric Isothermic Ensemble.....	15
2.2 trajectory Analysis.....	16
2.2.1 root mean square deviation (RMSD).....	16
2.2.2 root mean square fluctuation (RMSF).....	16

Chapter 3 Computational detail.....	18
3.1 Hardware	18
3.2 Software	18
3.3 Computational method	18
3.3.1 Construct an initial model method	18
3.3.2 Molecular dynamic simulation details	21
3.3.3 MD Trajectory analysis.....	21
Chapter 4 Result and Discussion	23
4.1 Structure stability and deviation.....	23
4.2 Conformational response of the pore-lining residues.....	27
4.3 Bilayer thickness.....	31
4.4 Asymmetric rearrangement of M2TM helices.....	32
REFERENCES	35
VITA.....	39

LIST OF TABLES

	Page
Table 1 Sample of know flu	2
Table 2 simulation systems, PBC dimension, total number of atoms, simulation time and number of independent runs	20
Table 3 Average RMSD value with respect to the starting structure.....	24
Table 4 The separation of diagonal subunit transmembrane helix calculated based on the α - α distances.....	26
Table 5 Membrane thickness measured from height of the density curve.....	31



LIST OF FIGURES

	Page
Figure 1 Structure of Influenza A Virus	2
Figure 2 The replication of influenza A	3
Figure 3 Tetramer structure of the transmembrane domain of M2.	4
Figure 4 Transmembrane segments of M2 channel at C-terminal	4
Figure 5 conformation of His37 at neutral pH condition.	5
Figure 6 A schematic representation of conformational changes of M2 channel from closed to open in response to lowering pH	6
Figure 7 Amantadine and rimantadine	6
Figure 8 The spin-labeling reaction.	7
Figure 9 ESR spectra and spin coupling values of N-terminal spin label side.....	8
Figure 10 Cartoon model show tilting M2 channel transmembrane segments due to different thickness transmembrane segment.....	9
Figure 11 Spin label site on the transmembrane segment protein of M2 channel....	10
Figure 12 spin label on cysteine	10
Figure 13 ESR spectra and spin coupling values of C-terminal spin label side.....	11
Figure 14 Cartoon model show tilting M2 channel transmembrane segments.....	11
Figure 15 Geometry of a simple chain molecule	14
Figure 16 schematic of periodic boundary condition in 2 dimensions.....	15
Figure 17 Simulation systems of the M2-DLPC, M2-DMPC and M2-POPC	19
Figure 18 Chemical structure of 3 different thickness (a) DLPC (b) DMPC (c) POPC ...	20
Figure 19 C α RMSDs over 100 ns simulation time.....	23

Figure 20 Structure comparison of snapshot representative structures of nine systems superimposed onto the x-ray structure.	24
Figure 21 Comparison of the C α - C α distances of the residues in diagonally opposite subunits.	26
Figure 22 Pore-lining residues	28
Figure 23 The normal distribution of the C α - C α distances of the pore-lining residues between diagonal subunits of M2, SL45 and SL45 _{fixed} model systems as a function of different bilayer thickness.	29
Figure 24 The NO-NO distances between diagonal subunits of SL45-DLPC, SL45-DMPC and SL45-POPC	30
Figure 25 The bilayer thickness estimated from the density profiles of nine MD systems	31
Figure 26 Cartoon representation of the four TMs rearrangement of the initial structure of the simulations.	33

Chapter 1

Introduction

1.1 Research rationale

Influenza or well known as flu occurs by infection from influenza virus. The flu virus attacks human respiratory by inhaling nasal droplets, saliva and sputum of infected persons. The influenza virus may be transmitted among humans in various ways, for instance coughing, sneezing, contact and sharing personal uses such as towels, glasses, phones etc.

Commonly, range of symptoms of the Influenza is more severe than the common cold. The symptoms of the influenza occur suddenly, while the symptoms of the cold occur gradually. Important symptoms of influenza are high fever for many days, especially in children with high fever, above 39-40 Celsius degrees for 3-4 consecutive days and may be accompanied by chills. In addition, older children and adults tend to have muscle aches, tired and bored with food.

There are four types of influenza virus that have been identified. They are categorized into type A, B, C and D. Especially, the Influenza A virus also can be divided into subtype based on the difference in the glycoproteins at the viral surface that are hemagglutinin (HA) [1] and neuraminidase (NA) [2]. There are 16 different HAs and 9 NAs. Influenza A subtype are named after these viral proteins, H(x)N(y), etc. Influenza B are not further divided into subtypes. Influenza C and D are rare compared to influenza A and B Table 1 shows the influenza A subtypes of known human pandemic deaths in the past.

Table 1 Sample of know flu

Subtype	Flu
H1N1	Spanish flu (1918), Swine Flu (2009)
H2N2	Asian Flu (1957)
H3N2	Hong Kong Flu (1968)
H5N1	Bird Flu (2004)

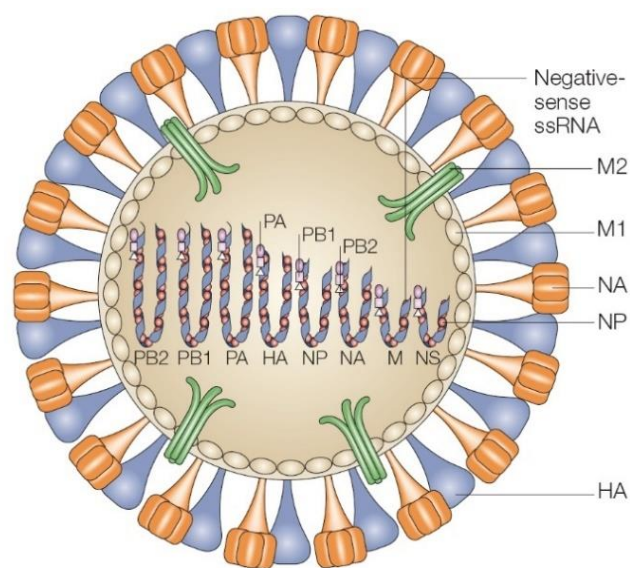


Figure 1 Structure of Influenza A Virus

In the viral life cycle, influenza A virus uses its HA to bind to salicylic acid receptor site located on host cell membrane. After HA binding, the virus enters to the host cell through endocytosis. During acidification in cytoplasm of the host cell, conformation change of the HA leads to the fusion between viral membrane and endosomal membrane. Under an acidic condition in cytoplasm, the His37 is protonated, inducing a conformational change of M2 to open the pore by opening the hydrophobic gate formed by Trp41. [3] As the Trp41 is opened, [4-5] proton flow into influenza A virus via M2 channel [6-7]. The pH change in the viral particle leads to the viral cell dissociation which releases all genetic materials of the virus. The genetic materials go into nucleus of the host cell for the genetic replication of the virus. [8] The replication process of the influenza viral life cycle is shown in Figure 2.

Adamantane and rimantadine [9] are two main drugs used to block the action of M2 channel. [10-11]

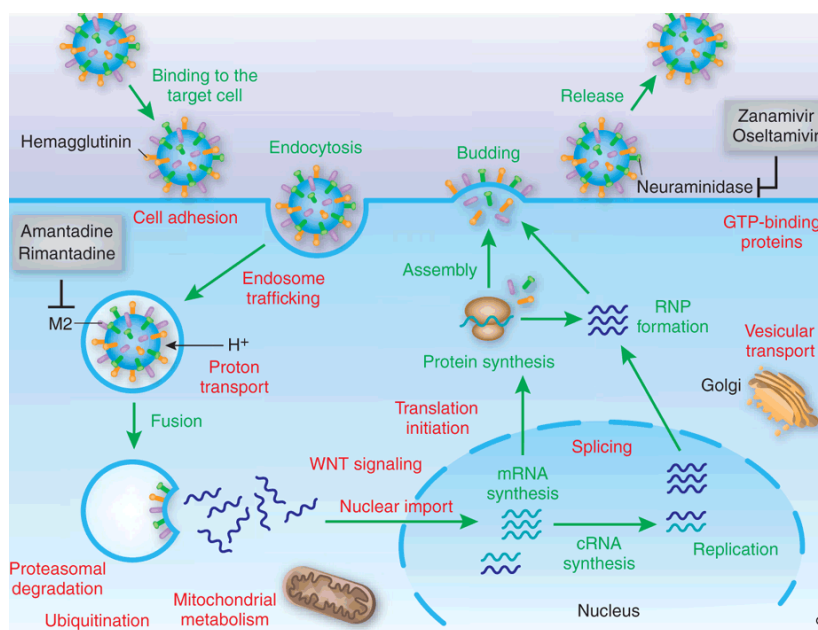


Figure 2 The replication of influenza A

Besides HA and NA located on the viral membrane, the matrix protein 2 (M2) plays an important role in virus replication. [12-13] [12-13] The M2 channel is a homotetrameric membrane protein which consists of 4 identical subunits (Figure 3). Each subunit consists of 97 residues. M2 consists of single transmembrane (TM) segment with 25 amino acid residues in length. The residue sequence in TM domain is Ser22-Ser-Asp-Pro-Leu-Val-Val-Ala-Ala-Ser-Ile-Ile-Gly-Ile-Leu-His37-Leu-Ile-Leu-Trp41-Ile-Leu-Asp-Arg-Leu46. The four transmembrane segments assemble to form a proton permeation pore. His37 acts as a pH sensor activated in acidic condition or low pH condition while Trp41 acts as a proton gate. [14] In the closed state, the Trp41 gate is stabilized by inter-subunit hydrogen bonding with Asp 44 (Figure 4).

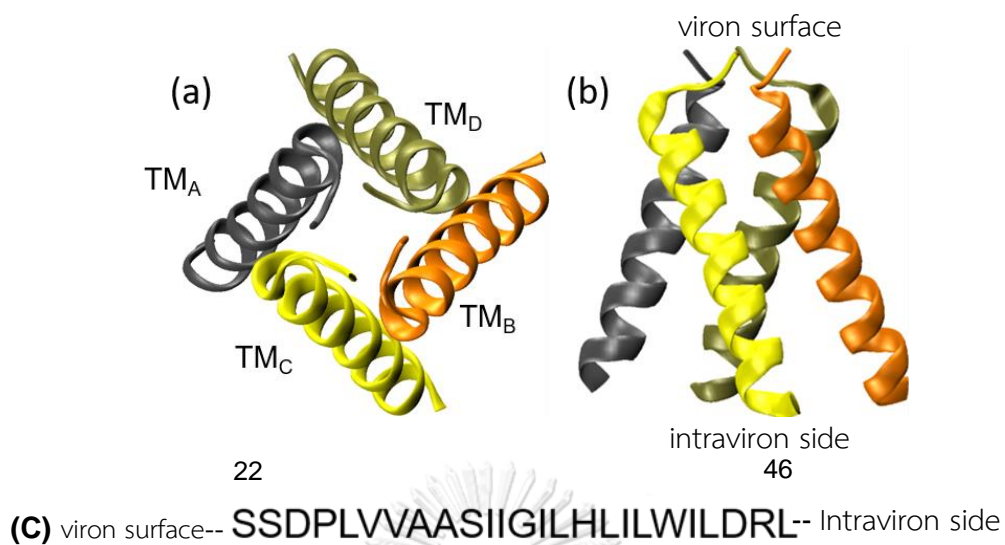


Figure 3 Tetramer structure of the transmembrane domain of M2.

(a) Extracellular view perpendicular to the four-fold axis.

Each TM segment is labeled as TM_A , TM_B , TM_C , and TM_D .

(b) Side view. (c) Amino acid sequence of M2 TM

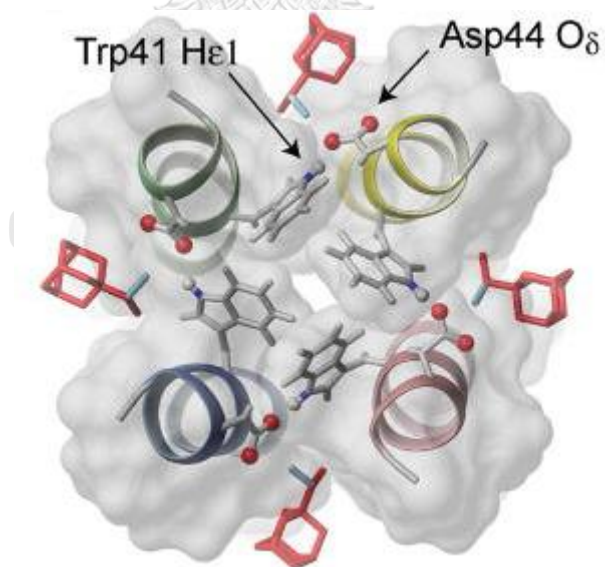


Figure 4 Transmembrane segments of M2 channel at C-terminal

At neutral pH condition, the conformation of His37 was proposed by energetics and dynamics comparison that had two alternative conformations of doubly protonated state (2 out of 4 of His37 are protonated). Those are dimer of dimer and histidine box (Figure 5). In the former, each dimer was proposed to form a low-barrier hydrogen bond with shared proton freely move between donor and acceptor. For the latter There are no direct hydrogen bonds between four His37. Each form hydrogen bonds with adjacent cluster of water molecules. [15]

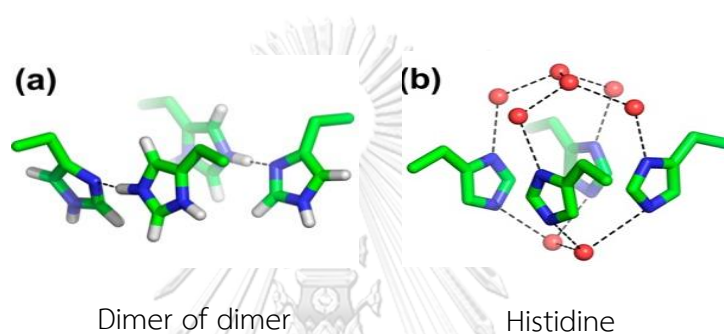


Figure 5 conformation of His37 at neutral pH condition.

(a) Dimer of dimer and (b) Histidine Box

At lower pH condition, His37 side chains are protonated. They repel each other by electrostatic interactions. As the result, the four TM segments are not stabilized in the closed conformation. This destabilization brakes hydrogen bond interaction between Trp41 and Asp 44, opening the hydrophobic gate of M2. As the pore opens, protons flux into the viral (Figure 6).[16]

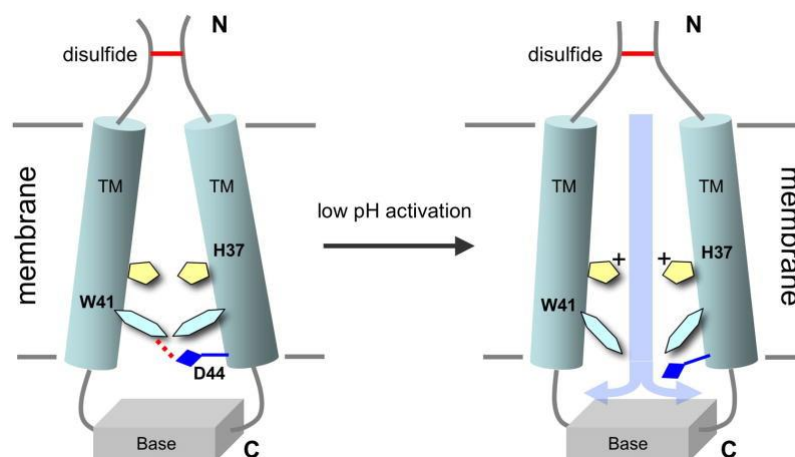


Figure 6 A schematic representation of conformational changes of M2 channel from closed to open in response to lowering pH

As described above, the M2 channel play an essential role for influenza A virus replication. Adamantane compound drugs, including Amantadine (1-aminoadamantan hydrochloride) and rimantadine (a-methyl-1-adamantane methylamine hydrochloride), have been used as an inhibitor for M2 Channel (Figure 7). They are used to block the proton conduction in M2. If His37 is not protonated, the M2 channel becomes more stable in the closed conformation. Hence, the Trp41 proton gate of the protein does not open. As a consequence, protons do not flow into the viral cell. The cell dissociation does not occur and there are genetic materials released from the virus into the host cell. Eventually, the virus replication does not happen. [17]

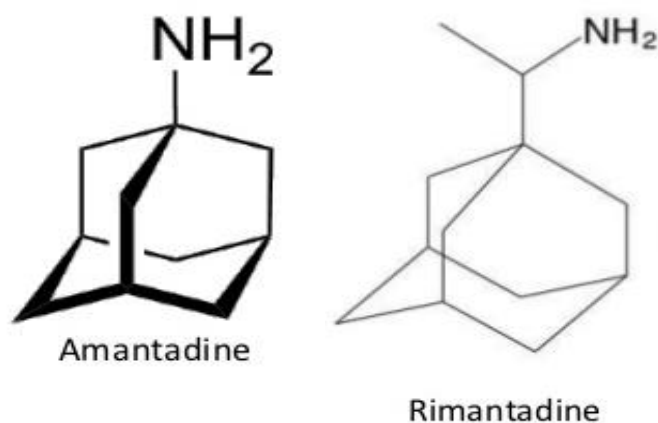


Figure 7 Amantadine and rimantadine

1.2 Literature review

Although there have been many studies about an effect of pH and inhibitors, on the M2 conformation, a few studies about interactions between M2 and lipid has been reported. As has been known, phospholipids play a significant role for membrane protein functions. Furthermore, thickness of a lipid bilayer can significantly affect the activity of membrane proteins. Bilayer thickness is directly related with the acyl chain lengths of phospholipid. In this study, we are interested about the influence of phospholipids to the orientation and structural stability of M2TM. We employed a MD simulation study of M2 in phospholipids with similar head groups but different acyl chain lengths. The results were interpreted by comparing with the experimentally measured spin label EPR data. Site-directed spin labeling in combination with electron paramagnetic resonance (SDSL-EPR) spectroscopy has been a powerful approach in the studies of membrane proteins in near native environment. SDSL-EPR employs pyrrolidine-based nitroxide spin label which is a stable free radical group (Figure 8). The nitroxide spin labeled agent can be specifically incorporated at the target site within proteins. SDSL-EPR is capable of providing structure and dynamics information of proteins with regard to developed experimental technique, Therefore, a review of literatures involved with a scope of the study is presented in this section

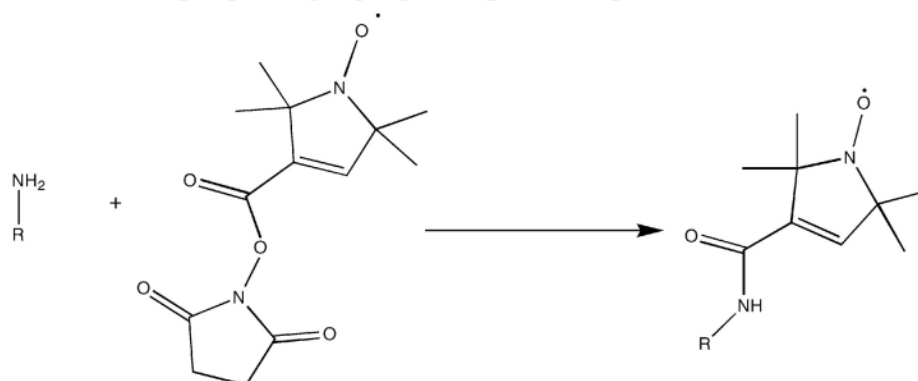


Figure 8 The spin-labeling reaction.

The reaction of 2,2,5,5-tetramethyl-3-pyrrolin-1-oxyl-3-carboxylic acid N-hydroxy succinimide ester to produce an N-terminal nitroxide labeled peptide.

In 2005, Krisna et al. [17] employed nitroxide spin labeled peptide attached at the position Ser22 of M2 TM segments. The spin label EPR were carried out by varying different phospholipids as follows: 1,2-dilauroyl-sn-glycero-3-phosphocholine (DLPC, C12:0), 1,2-dimyristoyl-sn-glycero-3-phosphocholine (DMPC, C14:0), 1,2-dimyristoyl-sn-glycero-3-phosphocholine (DOPC,18:1) and 1-palmitoyl-2-oleoyl-sn-glycero-3-phosphocholine (POPC,C16:0-18:1). Based on EPR data, they found that the length of hydrocarbon chain of phospholipids is related to the degree of nitroxide spin-spin couplings. Long-chain lipid gave the higher spin coupling value whereas short-chain lipid produced weaker spin-spin interactions. The spin-coupling interactions increases as the length of the lipid increase according to the following order: DLPC > DMPC > DOPC > POPC (Figure 9).

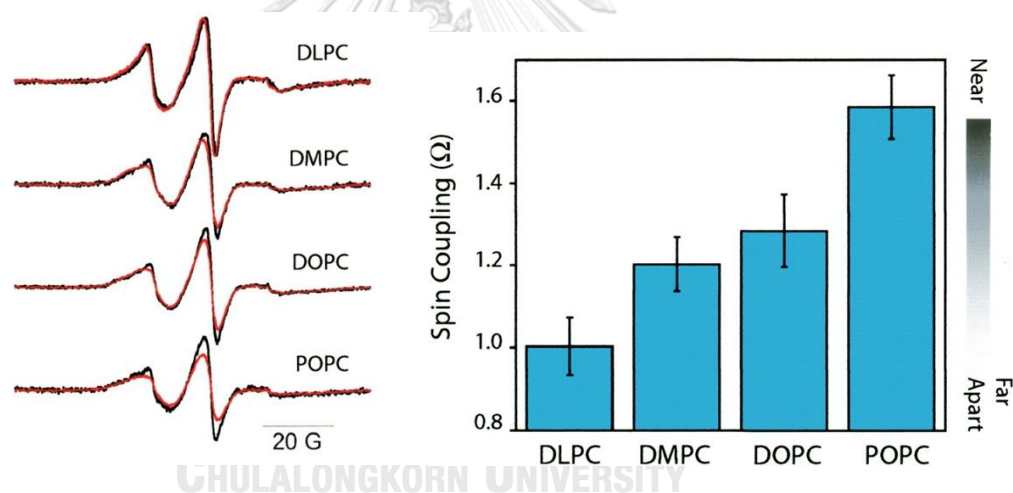


Figure 9 ESR spectra and spin coupling values of N-terminal spin label side

They had proposed that the transmembrane segments tilted for balancing hydrophobic part in phospholipid bilayer. The thicker phospholipid bilayer caused the transmembrane segment less tilted.

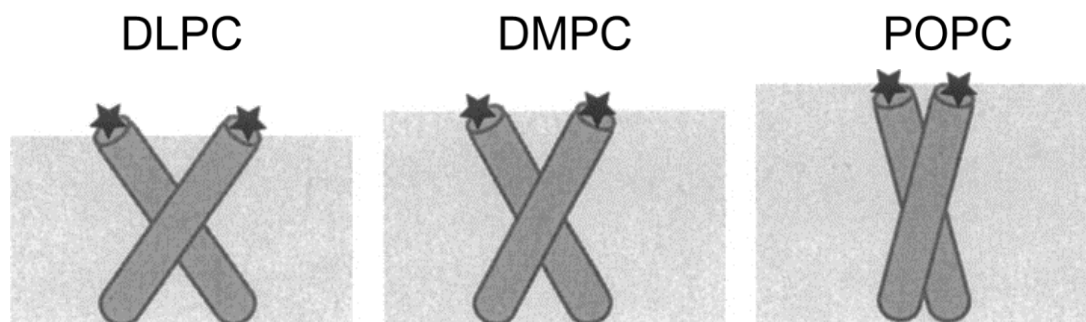


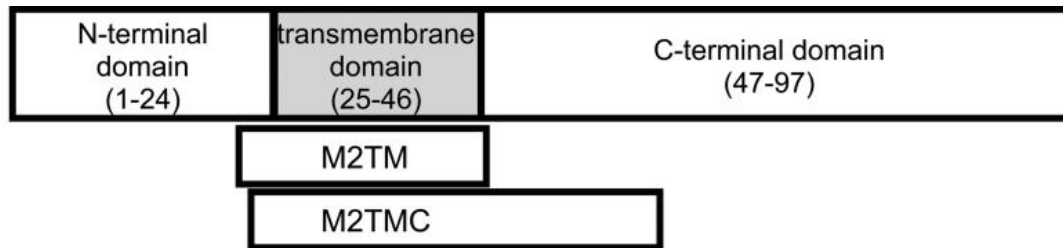
Figure 10 Cartoon model show tilting M2 channel transmembrane segments due to different thickness transmembrane segment.

Cylinders symbol the transmembrane segment.

2 of 4 segments are shown. Stars symbol N-terminal nitroxide labeled peptide.

Gray rectangular symbol phospholipid bilayer thickness.

The dependence of hydrophobic thickness on the M2TM conformational changes has been additionally demonstrated by Saotome et al. [18] They used EPR spin-label technique to investigate the change in M2TM conformation in different thickness phospholipid bilayers. In the study, they incorporated the spin label at Cys45 of M2TMC (Figure 11). with 1-oxy-2,2,5,5-tetramethylpyrroline-3-methyl-methanethiosulfonate (MTSSL) (Figure 12). A change in the global structure of M2 was interpreted from the EPR spectral amplitude, line broadening and spin-spin coupling (Figure 13). From a set of EPR spectra of the spin labeled M2TM reconstituted in three phospholipid bilayer constructs, a conformational change has been proposed based on changes in the spin coupling value. The study concludes that M2TM adapts to the membrane thickness by a helix tilt mechanism (Figure 14).



M2TM 22 46
 *SSDPLVVAASIIGILHLILWILDRL
 M2TMC R45C/C50S 23 60
 SDPLVVAASIIGILHLILWILDCLFFKS I YRFF EHGLK
 M2TMC C50S 23 60
 SDPLVVAASIIGILHLILWILDRLFFKS I YRFF EHGLK

Figure 11 Spin label site on the transmembrane segment protein of M2 channel. N-terminal spin label site is Ser22 (stared) on M2TM (M2 transmembrane). C-terminal spin label site is Cys45 (underlined) on M2TMC R45C/C50S (longer M2 peptide).

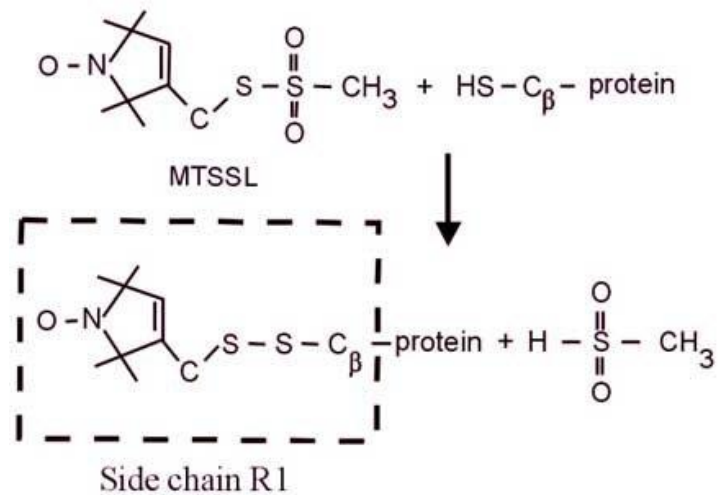


Figure 12 spin label on cysteine by using MTSSL, 1-oxyl-2,2,5,5-tetramethylpyrroline-3-methyl-methanethiosulfonate.

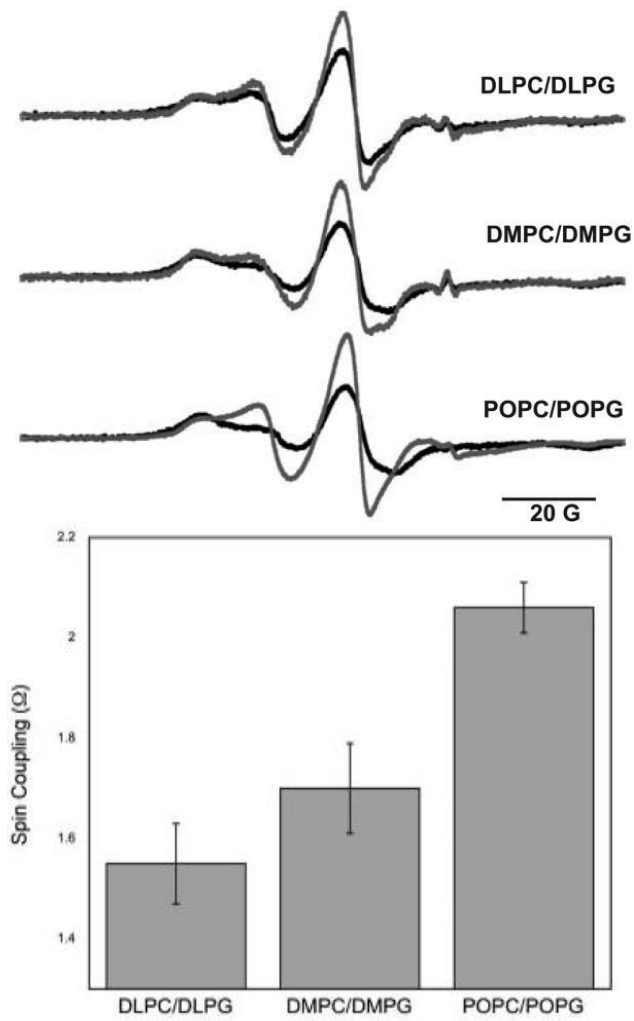


Figure 13 ESR spectra and spin coupling values of C-terminal spin label side

DLPC

จุฬาลงกรณ์มหาวิทยาลัย
CHULALONGKORN UNIVERSITY

DMPC

POPC

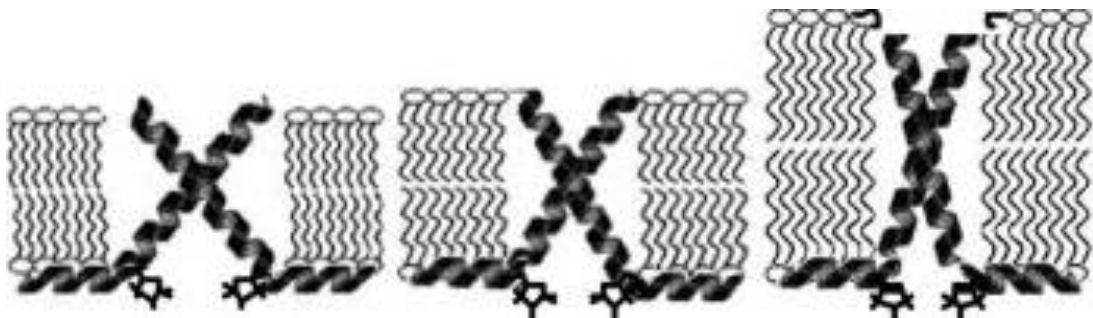


Figure 14 Cartoon model show tilting M2 channel transmembrane segments due to different thickness transmembrane. the Cys45 of M2TMC R45C/C50S were spin labeled. 2 of 4 segments are shown.

1.3 scope of this research

While the available structural data from EPR enable to characterize local environment and dynamics, it still remains technically challenging to atomic resolution structures. To interpret an effect of different membrane thickness on the M2TM conformation, we performed molecular dynamics (MD) simulation of the M2TM embedded in different lipid membrane; POPC (1-palmitoyl-2-oleoyl-sn-glycero-3-phosphocholine), DMPC and DLPC. The three phospholipid constructs are different in their acyl chain lengths which is defined by the number of carbons and saturation of fatty acids. POPC (C16:0, C18:1PC) contains 16 and 18 carbons with an unsaturated fatty acid. DLPC (diC12:0PC)) and DMPC (diC14:0PC) contains two saturated acyl chains of C12 and C14, respectively. We described the root-mean-square deviation (RMSD), the root-mean-square fluctuation (RMSF) and TM-TM distances to demonstrate an impact of membrane thickness on the conformation and flexibility of M2TM.

Chapter 2

Theory Background

2.1 MD Simulation

Computer simulation, such as molecular mechanics (MM) [19], Monte Carlo simulation (MC) [20] and molecular dynamic simulation (MD) [21] is used for study more detail that conventional experiment is limited. MD simulation is a computer simulation popularly used to study macro molecule or biological relevance, protein, drug, nucleic acid, lipid, carbohydrate etc. The MD simulation can be performed by NAMD [22], AMBER [23], GROMACS[24], etc. The MD simulation give time-dependent behavior of a molecular system. The simulation calculates base on Newton's equation of motion. Force of the particle calculated from second derivatives of the time and negative derivatives of potential energy. Where F_i is force, m_i is mass, r_i is position of atom i and V is potential function.

$$F_i = m_i \frac{\partial^2 r_i}{\partial t^2} = - \frac{\partial V}{\partial r_i}$$

Potential function is complex equation that represent force field on atom i : spring of bond length and angle, periodic function of bond rotation and Lennard-Jones potential and the Coulomb's law for van der Waals and electrostatic interaction [21, 25].

$$V_{potential} = \frac{1}{2} \sum_{bond} k_{ij}^r (r_{ij} - r_{eq})^2 + \frac{1}{2} \sum_{bend\ angles} k_{ijk}^\theta (\theta_{ijk} - \theta_{eq})^2 + \frac{1}{2} \sum_{torsion\ angles} \sum_m k_{ijkl}^{\phi, m} (1 + \cos(m\phi_{ijkl} - \gamma_m)) + 4\epsilon \sum_{atom} \left(\frac{\sigma}{r_{ij}} \right)^{12} - \left(\frac{\sigma}{r_{ij}} \right)^6 + \frac{1}{4\pi \epsilon_0} \sum_{atom} \frac{Q_i Q_j}{r_{ij}}$$

Where r is distance, r_{eq} is equilibrium distance, k^r stretching force constant, θ is angle, θ_{eq} is equilibrium angle, k^θ is bending force constant, ϕ is torsion angle,

k^ϕ is torsion angle force constant, γ is phase angle, ϵ is well deep, σ is diameter, ϵ_0 dielectric constant, and Q is atomic charge.

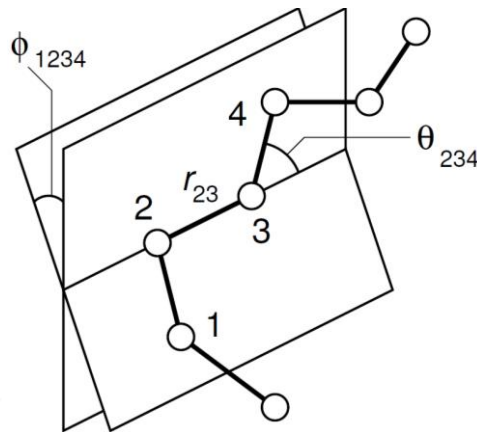


Figure 15 Geometry of a simple chain molecule

2.2.1 Integration algorithm

When particle change position, Force on the particle from potential function at each position. there is no analytical solution to solve this complication. Numerical methods must be used. Nanoscale Molecular Dynamics (NAMD) uses a multiple time stepping integration scheme by varlet algorithms. Varlet algorithms can be written as following equation.

$$r(t + \delta t) = 2r(t) - r(r - \delta t) + a(t)\delta t^2$$

Where r is the position and a is the acceleration (the second derivative with respect to time)

this algorithm uses positions and accelerations at time t and the positions from time $t - dt$ to calculate new positions at time $t + dt$. The algorithm uses no explicit velocities. The advantage are straightforward and modest storage requirements. The disadvantage is moderate precision algorithm.

2.1.2 Periodic boundary conditions

Periodic boundary conditions are a set of boundary condition using finite system or unit cell to represent infinite system

The gray square is primary unit cell. The white squares are images replicated from primary unit cell. While an atom goes outside of the primary unit cell to the image, an image atom come inside to the primary unit cell

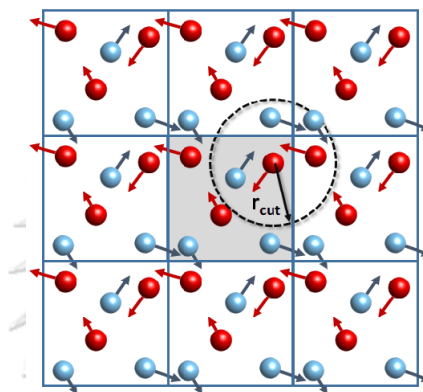


Figure 16 schematic of periodic boundary condition in 2 dimensions

2.1.3 Cutoff

From periodic boundary condition, there are images of atom, no more one image of the atom non-bounded interact with others. Cutoff radius, R_c or r_{cut} is defined must not exceed half of the shortest of box vector $R_c < \min(\|a\|, \|b\|, \|c\|)$

2.1.4 Isobaric Isothermic Ensemble

The state of a classical system can be completely described by specifying the positions and momenta of all particles.[26] A statistical ensemble is a collection of various microstates of an equilibrium macroscopic systems. The systems have different microscopic states, but they have an identical macroscopic or thermodynamic state. The systems determined by the constraints operating on the system.

Isobaric isothermic ensemble is popular ensembles as most of the real experiments are carried out under controlled conditions of temperature and pressure. the volume of the system can fluctuate at constant pressure and the energy is computed for new configurations. In other words, the ensemble is characterized by a fixed number of atoms, N , a fixed pressure, P , and a fixed temperature, T . So, this ensemble is called NPT ensemble.[27-28]

2.2 trajectory Analysis

Output from molecular dynamic simulation is trajectory. There are many ways to analyze data. In this research, we used root mean square deviation (RMSD), root mean square fluctuation (RMSF) and distance between some residue on the M2 Transmembrane segments.

2.2.1 root mean square deviation (RMSD)

RMSD of certain atoms in a molecule with respect to reference structure, r_i^{ref} , is calculated as

$$RMSD(t) = \left[\frac{1}{M} \sum_{i=1}^N m_i |r_i(t) - r_i^{ref}|^2 \right]^{1/2}$$

Where $M = \sum_i m_i$ and $r_i(t)$ is the position of atom i at time t after least square fitting the structure to reference structure

2.2.2 root mean square fluctuation (RMSF)

RMSF is a measure of the deviation between the position of particle i and some reference position

$$RMSF_i = \left[\frac{1}{T} \sum_{t_j=1}^T |r_i(t_j) - r_i^{ref}|^2 \right]^{1/2}$$

where T is the time over which one wants to average and r_i^{ref} is the reference position of particle i . Typically this reference position will be the time-averaged position of the same particle i , i.e., $r_i^{ref} = \bar{r}_i$



Chapter 3

Computational detail

3.1 Hardware

Workstation Computers located at The Center of Excellence in Computational Chemistry (CECC), Department of Chemistry, Faculty of Science, Chulalongkorn University

3.2 Software

NAMD 2.12, NANoscale Molecular Dynamics program, developed by the Theoretical and Computational Biophysics Group in the university of Illinois at Urbana-Champaign. This program is used for performing MD simulation [22]

VMD 1.9.3, Visual Molecular Dynamics, is used with NAMD. VMD is used for visualizing, modeling and analyzing biomolecular system for MD simulation. [29]

CHARM, Chemistry at Harvard Molecular Mechanics is a MD program, contain force field parameter for bio molecules, protein, carbohydrate, nucleic acid etc. It is used to calculate potential energy in performing MD simulation. [30]

Wordom, multifunction software, can be used for analyzing MD trajectories such as secondary structure, calculation of protein structure network, RMSF etc. [31]

3.3 Computational method

3.3.1 Construct an initial model method

Initial structure of M2 channel tetramer was taken from the crystal structure of influenza A M2 wild type TM domain (strain A/Udm/307/1972 H3N2) with PDB code 4QK, at high pH, closed-state channel. Missing hydrogen atoms were generated by PSFGEN, VMD authorized plugin. PROPKA was used to assign protonation states of ionizable residues at neutral pH. In addition, site-direct spin was performed by MTSSL spin labeling on Cys45 following pervious study.

Protein-membrane systems were set by following membrane protein tutorial. M2 Channel was embedded in three different phospholipid bilayers, DLPC (1,2-dilauroyl-sn-glycero-3-phosphocholine), DMPC (1,2-dimyristoyl-sn-glycero-3-phosphocholine) and POPC (1-palmitoyl-2-oleoyl-sn-glycero-3-phosphocholine). Then each M2-lipid system was solvated with TIP3P water molecules. The three simulation systems are denoted as follows: M2-DLPC, M2-DMPC and M2-POPC.

In addition, the simulations were performed by varying three different conditions; unlabeled M2, spin labeled M2 at residue position 45 (denoted as SL45) and terminal constrained SL45 (denoted as SL45_{fixed}). For SL45_{fixed}, the simulations were carried out by constraining the position of both N- and C-terminal residues, (Ser22 and Leu46 respectively) in order to take into account, the terminal-end effect. A total of nine simulation systems carried out in this study was shown in Table 2.

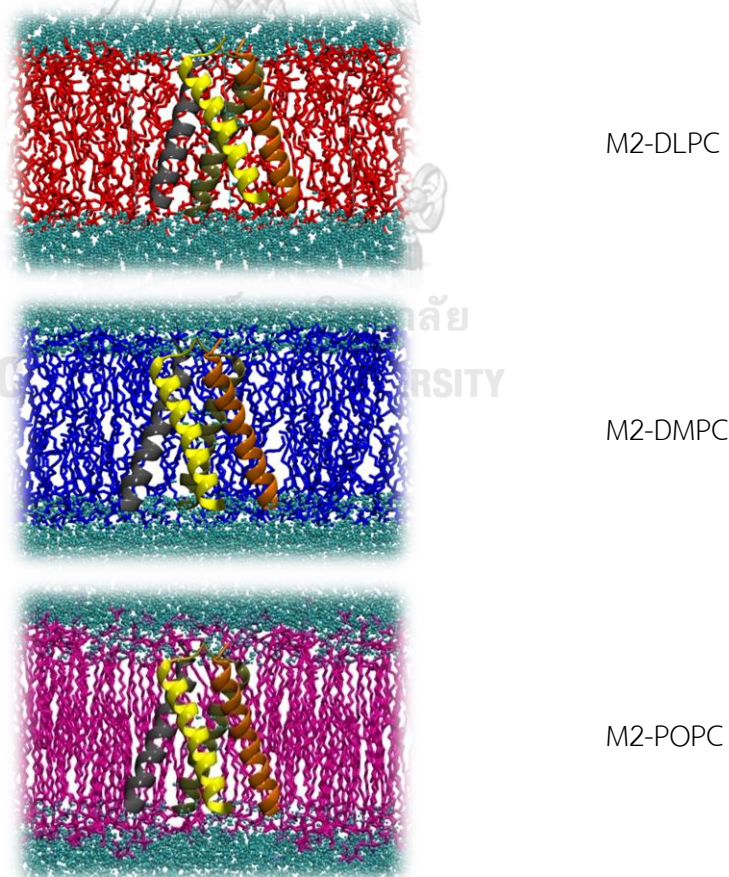


Figure 17 Simulation systems of the M2-DLPC, M2-DMPC and M2-POPC

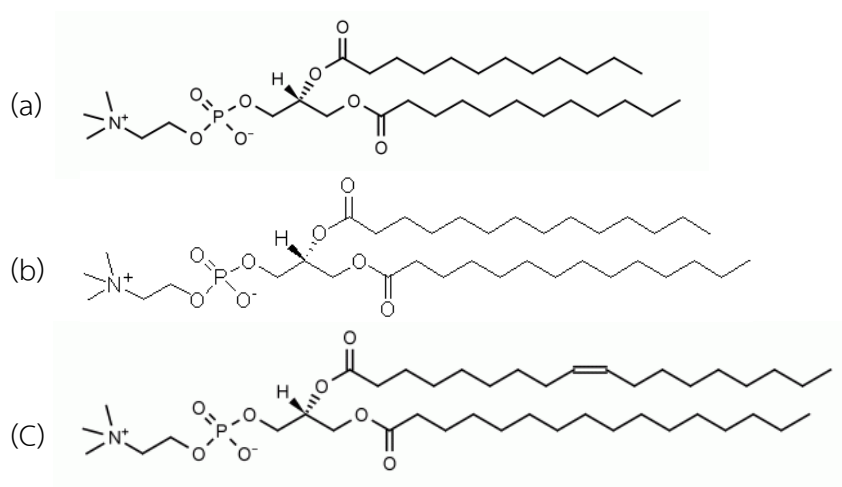


Figure 18 Chemical structure of 3 different thickness (a) DLPC (b) DMPC (c) POPC

Table 2 simulation systems, PBC dimension, total number of atoms, simulation time and number of independent runs

System	Box dimension (Å)	total atom	time (ns) × repetition
M2-DLPC	91×91×80	47559	100 × 5
M2-DMPC	97×98×88	57567	100 × 5
M2-POPC	96×96×88	61650	100 × 5
SL45-DLPC	89×89×89	50183	100 × 5
SL45-DMPC	100×100×90	63420	100 × 5
SL45-POPC	96×96×88	61956	100 × 5
SL45 _{fixed} -DLPC	89×89×89	50183	100 × 1
SL45 _{fixed} -DMPC	100×100×90	63420	100 × 1
SL45 _{fixed} -POPC	96×96×88	61956	100 × 1

3.3.2 Molecular dynamic simulation details

All M2-membrane systems were performed 100ns with time step 2 fs by NAMD software. CHARMM force field was applied for protein, lipid molecule metal ion. TIP3P model was used for water molecule. The force field parameters of the nitroxide spin label developed by Sezer et al. [32] were obtained from CHARMM-GUI web server. Charge of system was neutralized by 0.1 M NaCl. Systems were performed at 300 K and 1 atm. Langevin temperature and Langevin piston pressure coupling schemes were used [33-34]. Short-range interactions were calculated using a cutoff distance of 12 Å, and particle mesh Ewald method was used for long-range electrostatic interactions [35]. To pre-equilibrate the systems, a cycle of MD simulations was employed by restraining the protein structure with the force constant of the restrained harmonic potential decreasing from 1 to 0.1 kcal/(mol Å²). Subsequently, MD simulations were performed under NPT ensemble with a time step of 2 fs. Each snapshot was stored at every 1 ps in the trajectory. 100ns MD simulations were conducted with a time step of 2fs. The simulated systems were constructed using TCL scripts in VMD 1.9.3.

3.3.3 MD Trajectory analysis

All Trajectory from MD simulation were analyzed by modified VMD scripts. Unless otherwise specified, analysis of MD trajectories was carried out during the last 20 ns simulation. This was primarily to make sure that the systems had reached thermodynamic equilibrium and that structural features extracted from the trajectory were adequately characterized with least deviation. C α root mean square deviation (RMSD) was used for analyzing equilibrium or stability of the system. Averaged C α root mean square fluctuation (RMSF) over last 20 ns was used for analyzed fluctuation of individual amino acid residue. Superimposed snapshot, distribution of C α - C α distance of some amino acid residues of backbone and spin-spin distance were calculated for analyzing conformational change of the M2 channel in different

phospholipid bilayer types and conditions. The mass density of lipids was computed by searching lipid atoms along the membrane z-axis in the simulation box. The mass density profiles were obtained by employing adjacent-average smoothing of the density data with a window of 20. The tilt angle of each transmembrane segment is computed from the MD trajectories by defining the angle between the axis of the transmembrane helix and the axis of bilayer normal.



Chapter 4

Result and Discussion

4.1 Structure stability and deviation

The C α -RMSD respect to the initial structure was used to demonstrate structural equilibrium of the protein. The RMSD profiles were plotted and shown in Figure 20. In the beginning of the simulation, the C α -RMSD of all nine systems increases dramatically and reach equilibrium. At this stage, the global structure of M2 fluctuates very little with respect to their own average throughout 100ns simulations. The C α -RMSDs in all the equilibrated production trajectories kept stable within 2.0-3.0 Å for non-constrained simulations and within 0.8-2.0 Å for terminal constrained M2. The average C α -RMSDs in all the equilibrated production trajectories kept stable within 2.0-3.0 Å for non-constrained simulations and within 0.8-2.0 Å for terminal constrained M2. The average C α -RMSD values of the nine simulation systems were summarized in Table 3. It appears that the average C α -RMSD values of unlabeled M2 systems were not significantly different from those of SL45. This suggested that attaching the spin label into the protein did not severely affect overall structural dynamics of M2. For the SL45_{fixed} simulation systems, the movement of the backbone of M2 is restricted as shown by a lower C α -RMSD. The RMSD results indicate the overall stability of the structure for all studied systems during the simulations.

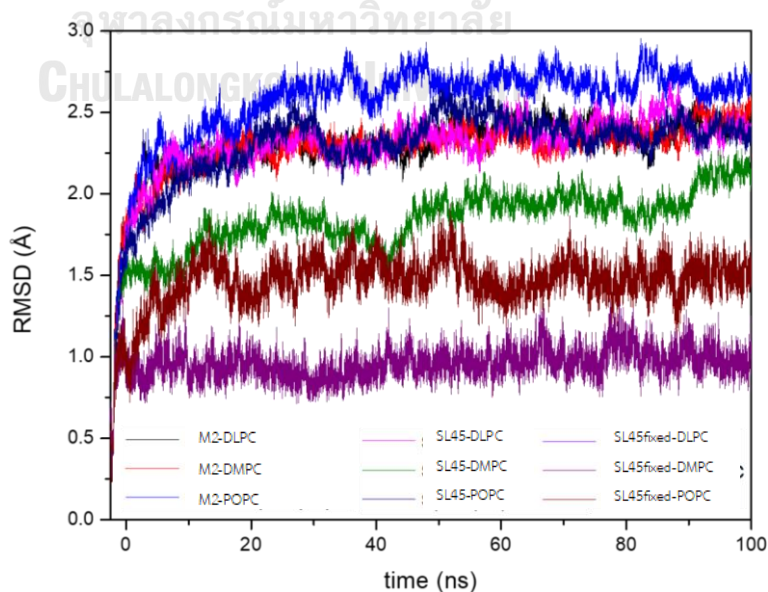


Figure 19 C α RMSDs over 100 ns simulation time

Table 3 Average RMSD value with respect to the starting structure

lipid	Average RMSD \pm SD (\AA)		
	M2	SL45	SL45 _{fixed}
DLPC	2.40 \pm 0.07	2.43 \pm 0.08	1.50 \pm 0.09
DMPC	2.42 \pm 0.07	2.00 \pm 0.12	1.00 \pm 0.08
POPC	2.69 \pm 0.07	2.38 \pm 0.06	1.50 \pm 0.09

Furthermore, the C α -RMSD values indicate the deviation of the global structure of the protein backbone with respect to the initial structure. From the simulation data, the average C α -RMSD were 2.40, 2.42 and 2.69 \AA for M2-DLPC, M2-DMPC and M2-POPC. The SL45-DLPC, SL45-DMPC and SL45-POPC exhibited the average C α -RMSD of 2.43, 2.00 and 2.38 \AA , respectively. The SL45_{fixed}-DLPC, SL45_{fixed}-DMPC and SL45_{fixed}-POPC showed the average C α -RMSD of 1.50, 1.00 and 1.50 \AA , respectively. As can be seen, the unlabeled M2 and SL45 systems exhibited a larger C α -RMSD than the SL45_{fixed} systems (Table 3). This indicated that the structures of the unlabeled M2 and SL45 significantly deviated from the x-ray structure whereas a minimum structure deviation was observed for the SL45_{fixed} systems. Backbone structure deviation between the MD snapshot structures of the nine systems and the x-ray structure were shown in Figure 20.

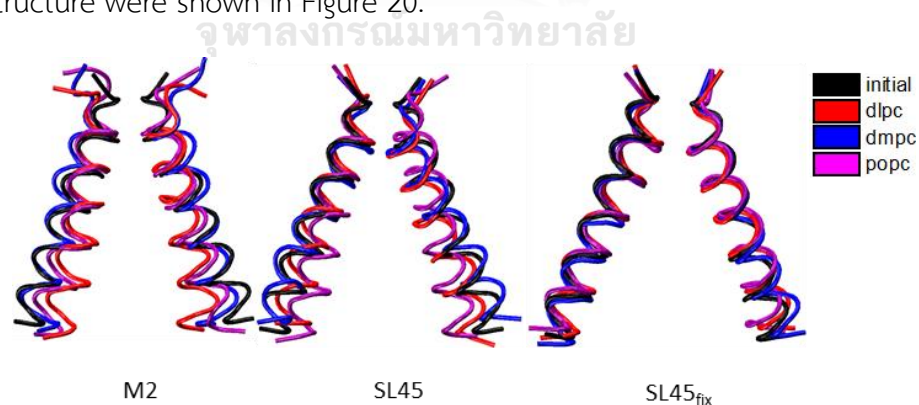


Figure 20 Structure comparison of snapshot representative structures of nine systems superimposed onto the x-ray structure.

A smallest deviation was observed for SL45_{fixed} systems.

To give a clear view of the structural change in response to phospholipid modification, the average $C\alpha$ - $C\alpha$ distances of the residues in diagonally opposite subunits are shown in Figure 19 and summarized in Table 3. In the initial x-ray structure, the distance separations between diagonal transmembrane helices were 7.87 (Ser23) and 22.60 (Arg45) Å for the residues near extracellular side and intracellular side of M2TM, respectively. Over simulation time, the distance separation increases at the extracellular side (12.5-14.9 Å for Ser23) whereas it decreases at the intracellular side (16.2-17.8 Å for Arg45) for the unlabeled M2 systems. Therefore, the effect of different acyl chain lengths on the M2TM structure was not clearly distinguishable. In other words, M2-DLPC, M2-DMPC and M2-POPC gave a similar impact on structural response of M2TM.

For the SL45 systems, structure changes of M2TM in response to the modification of phospholipid alkyl chain lengths were found to be slightly different from the unlabeled M2 system. The degree of $C\alpha$ - $C\alpha$ distance changes at the extracellular side of M2TM was smaller with a range of 10.6-12.2 Å for Ser23 but the intracellular M2TM exhibited a large variation of structure changes (from 20.7 to 29.2 Å for Arg45). It appears that the SL45-POPC was most sensitive to change in TM arrangement at the intracellular side whereas the SL45-DMPC was minimally influenced by the lipid modification. In the case of the terminal constrained simulation (the SL45_{fixed} systems), there was no significant impact in the global arrangement of the M2TM structure by the lipid modification. The arrangement at both end of TM helices was essentially unchanged with respect to the x-ray structure.

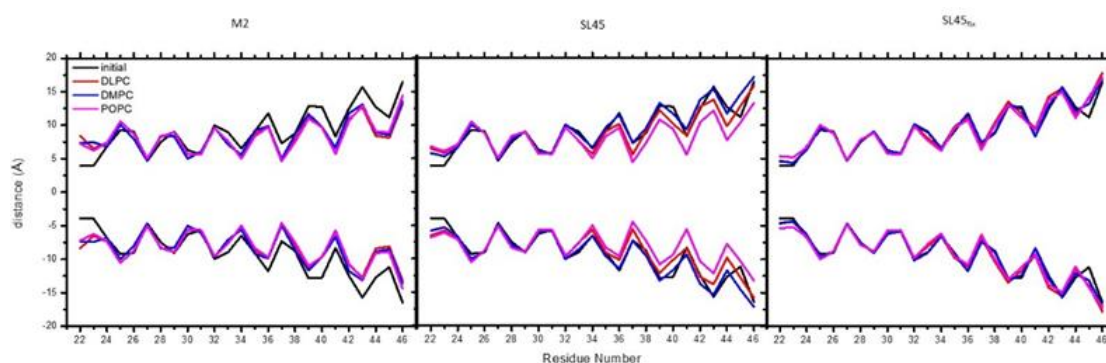


Figure 21 Comparison of the $C\alpha$ - $C\alpha$ distances of the residues in diagonally opposite subunits.

Table 4 The separation of diagonal subunit transmembrane helix calculated based on the $C\alpha$ - $C\alpha$ distances

Residue position	The $C\alpha$ distance separation of residues between diagonal subunits									
	x-ray	M2			SL45			SL45 _{fixed}		
		DLPC	DMPC	POPC	DLPC	DMPC	POPC	DLPC	DMPC	POPC
22SER	7.85	16.82	14.70	14.48	13.03	11.61	13.59	9.16	9.36	10.78
23SER	7.87	13.03	14.89	12.45	11.63	10.61	12.18	8.86	8.62	10.44
24ASP	13.68	14.75	13.59	14.67	13.99	13.30	14.23	12.82	12.60	13.39
25PRO	18.49	21.14	20.1	21.12	20.65	20.05	21.02	19.45	19.3	20.05
26LEU	18.18	17.41	15.99	17.51	17.58	17.63	17.52	17.6	17.71	17.71
27VAL	9.33	10.03	9.32	10.06	9.89	9.56	10.16	9.34	9.37	9.56
28VAL	14.97	16.67	16.83	16.56	16.32	15.87	16.71	15.3	15.3	15.76
29ALA	18.12	17.87	16.62	17.83	17.83	18	17.99	17.82	18.16	17.72
30ALA	12.56	11.33	10.03	11.29	11.37	11.9	11.47	11.78	12.37	11.46
31SER	11.32	11.36	12.13	11.3	11.36	11.69	11.3	11.41	11.7	11.38
32ILR	19.97	19.32	19.31	19.18	19.41	20.19	19.18	19.87	20.34	19.64
33ILE	17.99	15.22	14.25	15.35	15.12	17.1	15.35	16.17	18.13	15.41
34GLY	13.01	10.47	11.18	10.01	11.42	13.22	10.03	13.02	13.19	12.4
35ILE	18.18	17.27	18.37	16.66	18.18	19.33	16.64	19.61	18.74	19.19
36LEU	23.58	19.77	19.74	19.46	20.32	22.95	19.24	22.3	23.59	21.64

37HIS	14.59	9.52	9.86	9.22	11.19	14.64	8.89	13.47	14.82	12.66
38LEU	17.58	15.73	17.3	15	18.3	19.15	14.72	20.79	17.88	20.06
39ILE	25.71	22.49	23.38	21.99	24.39	26.56	21.66	27.04	26.1	26.09
40LEU	25.52	19.26	19.45	19.42	20.38	23.43	18.82	23.38	24.88	22.32
41TRP	16.68	11.72	13.31	11.45	16.83	18.78	11.18	18.9	16.63	18.6
42ILE	24.94	21.77	23.59	21.31	25.5	27.54	20.81	28.54	25.89	27.59
43LEU	31.43	25.41	26.25	25.91	27.61	30.79	24.37	30.99	31.21	29.87
44ASP	25.42	16.84	17.80	18.17	19.67	23.46	15.53	23.09	24.28	22.17
45ARG	22.60	16.25	17.04	17.84	25.64	29.22	20.73	27.98	26.31	28.50
46LEU	32.95	26.48	27.19	28.78	31.70	34.41	26.58	35.63	34.00	34.36

4.2 Conformational response of the pore-lining residues

To investigate the effect of phospholipid modification on the motion of transmembrane helices, we determined the distribution of the C α -C α diagonal distance of the pore-lining residues including Val27, Ser31, Gly34, His37 and Trp41 (Figure 22). From the simulations of nine systems, significant changes of distance separation among these residues with respect to the initial structure were observed indicating a rearrangement of transmembrane helices of M2. For Val27 and Ser31, an increase in the C α -C α distance were also observed for all nine simulated systems. This implies that the extracellular half of TM helices moves further away with respect to the initial structure. On the other hand, the C α -C α distance separation of Gly34 became shorter for all nine simulated systems, indicating that the mid of TM helices was likely to move closer as compared to the initial model. A discrepancy of the MD results among the nine simulated systems became more apparent at the intracellular half of the TM helices. In the case of M2 simulated in the DLPC, DMPC POPC bilayers, the C α -C α distances between the pore-lining residues for His37 and Trp41 were shorter with respect to the x-ray structure. Although an impact of the lipid acyl chain length on the distance changes of the residues for the intracellular half was in the same trend, conformational dynamics appear to be different. As can

be seen, the range of the C α -C α distance distribution for His37 and Trp41 goes from narrow to broad shape in the following order: M2-POPC < M2-DMPC < M2-DLPC. This suggested that backbone dynamics at His37 and Trp47 increase as a decrease in the acyl chain length. However, an effect of attaching spin label at residue position 45 gave results different from those of the M2 simulated systems. In case of the terminal unconstrained simulations (the SL45 system), His37 and Trp41 became closer in the C α -C α distances for SL45-POPC whereas they move further away for SL45-DMPC, as compared to the initial structure. Nevertheless, the C α -C α distances of His37 and Trp41 were observed to be increased in a similar manner for the terminal constrained simulations (SL45_{fixed}) with three different phospholipids.

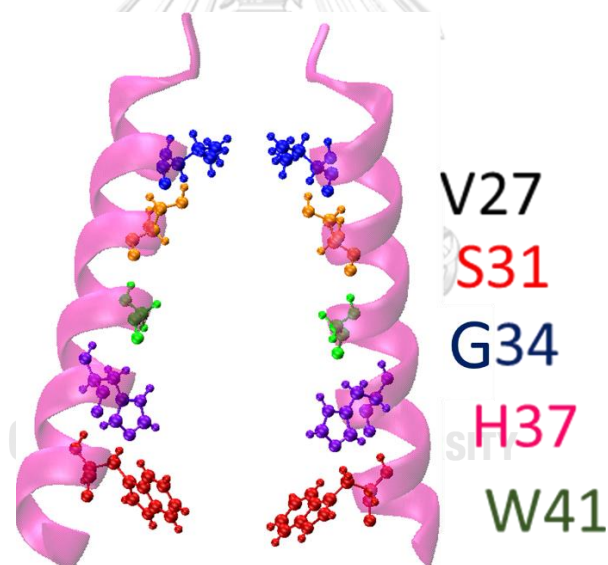


Figure 22 Pore-lining residues

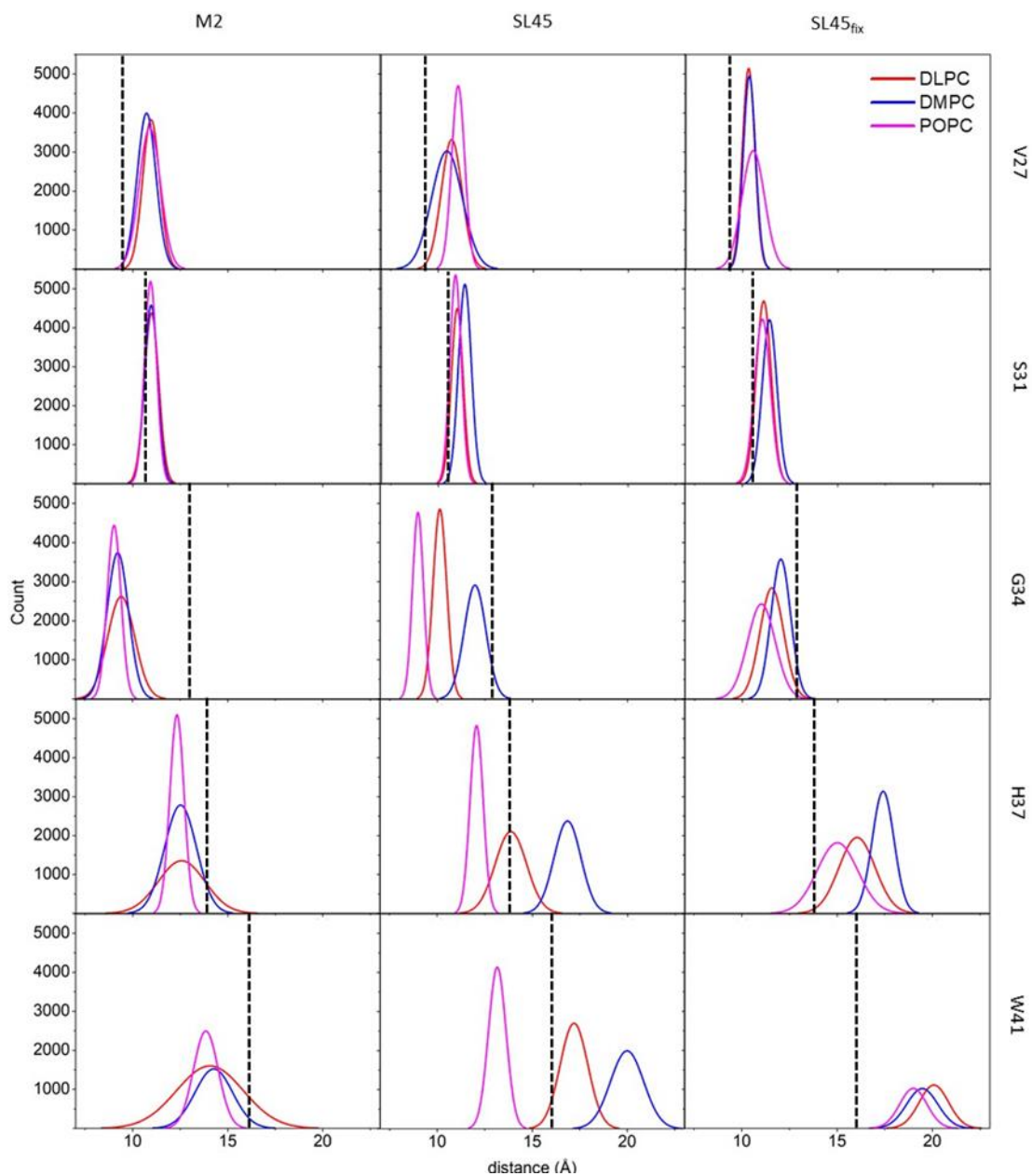


Figure 23 The normal distribution of the $C\alpha$ - $C\alpha$ distances of the pore-lining residues between diagonal subunits of M2, SL45 and SL45_{fixed} model systems as a function of different bilayer thickness. Dashed lines indicate the distance measured from the initial structure.

Figure 24 shows the inter subunit spin-spin distances obtained from the nine simulated systems. A shorter distance between the nitroxide groups of diagonal subunits was observed for SL45-POPC in comparison with SL45-DLPC and SL45-DMPC. This observation was consistent with the results summarized from the observation of the distance changes for the Trp41 residue in the SL45 simulated system. In addition, the MD results of SL45-POPC and SL45-DMPC systems were in good agreement with the spin-spin coupling data obtained from EPR experiments. From the overall results described above, we have concluded that the effect of the hydrophobic chain length in phospholipid has led to conformational changes of M2TM. The intracellular half of four TMs moves closer toward each other as the acyl chain length of the phospholipid is longer.

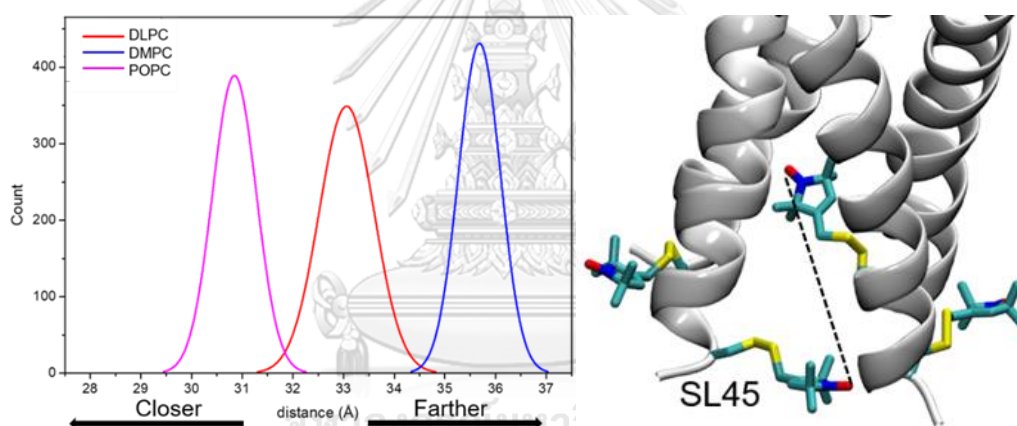


Figure 24 The NO-NO distances between diagonal subunits of SL45-DLPC, SL45-DMPC and SL45-POPC

The distances were measured between the nitroxide group of spin label side chain attached at residue position 45 of each TM.

4.3 Bilayer thickness

Thickness of phospholipid bilayer can affect the orientation of transmembrane proteins. Bilayer thickness was estimated by calculating the mass density of lipids in the simulation box. The mass density profile of the lipids across the bilayer illustrates how mass is distributed along the membrane z-axis. Figure 25 shows typical mass density profiles of hydrated protein-membrane systems. The zero-lipid density indicates water regions whereas the high lipid density corresponds to the lipid chain. The lipid density increases rapidly at the beginning of the upper and lower leaflets. We used the width at the half height of the density profile to estimate bilayer thickness. The bilayer thickness of M2-lipid bilayer systems increases in the following order: M2-DLPC < M2-DMPC < M2-POPC. A similar trend of the relation of the bilayer thickness was also observed for the SL45 and SL45_{fixed} simulated systems. The MD results have confirmed that the longest POPC has the most thickness whereas the shortest DLPC has the thinnest bilayer.

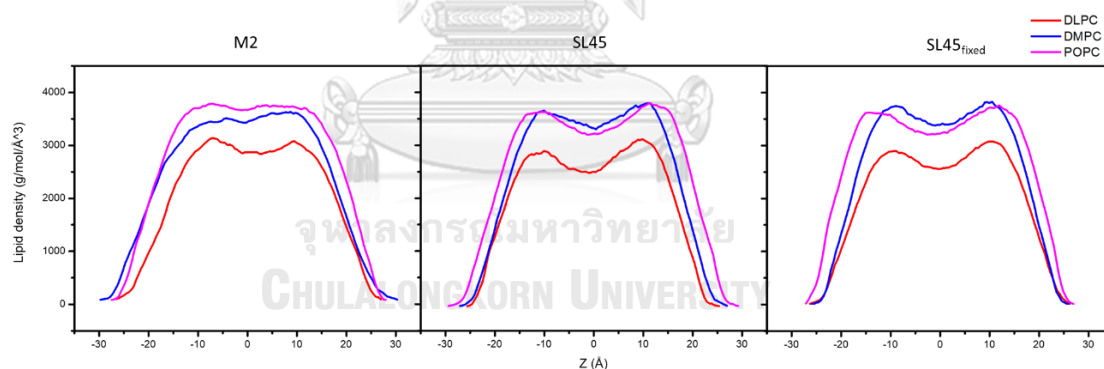


Figure 25 The bilayer thickness estimated from the density profiles of nine MD systems

Table 5 Membrane thickness measured from height of the density curve

lipid	Membrane thickness (Å)		
	M2	SL45	SL45 _{fixed}
DLPC	27.9	26.9	27.6
DMPC	30.4	28.2	28.1
POPC	31.8	31.3	31.5

4.4 Asymmetric rearrangement of M2TM helices

For a quantitative analysis of the conformational changes observed for M2TM, we have determined the orientation of four TMs by measuring a tilt angle of the TM helical axis with respect to the bilayer normal. The tilt angle of TM segments revealed the different influence of lipid acyl chain lengths on the conformational rearrangement of M2 channel as shown in Figure 26.

We found that the tetramer in M2-DLPC tilts slightly toward the bilayer normal in comparison with the initial orientation (with tilt angles of $\sim 30^\circ$ - 32°) as shown by a decrease in tilt angles at the maximum distribution peak ($\sim 25^\circ$ - 32°). On the other hand, 3 out of 4 TMs in SL45-DLPC move away from the bilayer normal (or the reference orientation shown in grey area in Figure 26) with measured tilt angles of $\sim 35^\circ$ - 40° while the remaining one TM moves toward the bilayer normal (tilt angle of $\sim 25^\circ$). This suggested that symmetry breaking of the tetramer was observed. In case of SL45_{fixed}-DLPC, the tetramer moves away from the bilayer normal and the fourfold symmetric arrangement of TMs was considerable unaltered. The tilt angles of the four TMs in SL45_{fixed}-DLPC were ($\sim 35^\circ$ - 38°).

For the simulations in DMPC lipid system, asymmetric TM rearrangement was observed for M2-DMPC. The tilt angles of four TMs at the maximum distribution were $\sim 20^\circ$, $\sim 23^\circ$, $\sim 30^\circ$, and $\sim 36^\circ$, indicating that two TMs were tilted closer to the bilayer normal, but one TM was tilted away from the bilayer normal. In contrast, the structural rearrangement of TMs in SL45-DMPC showed the TMs were tilted away from the initial orientation (tilt angles of $\sim 32^\circ$, $\sim 34^\circ$, $\sim 36^\circ$, and $\sim 40^\circ$). For the SL45_{fixed}-DMPC system, there was no significant change in structural rearrangement. The tilt angles of the four TM2 were spread in a narrow range from $\sim 29^\circ$ to 34° .

The asymmetric reorientation of TMs was found for the simulation of M2-POPC. The TMs move toward the bilayer normal with tilt angles of $\sim 22^\circ$, $\sim 27^\circ$, $\sim 28^\circ$, and $\sim 32^\circ$. For SL45-POPC, no significant rearrangement of the four TMs was found.

However, SL45_{fixed}-POPC showed a structural change in such a way that TMs were tilted away from the initial orientation.

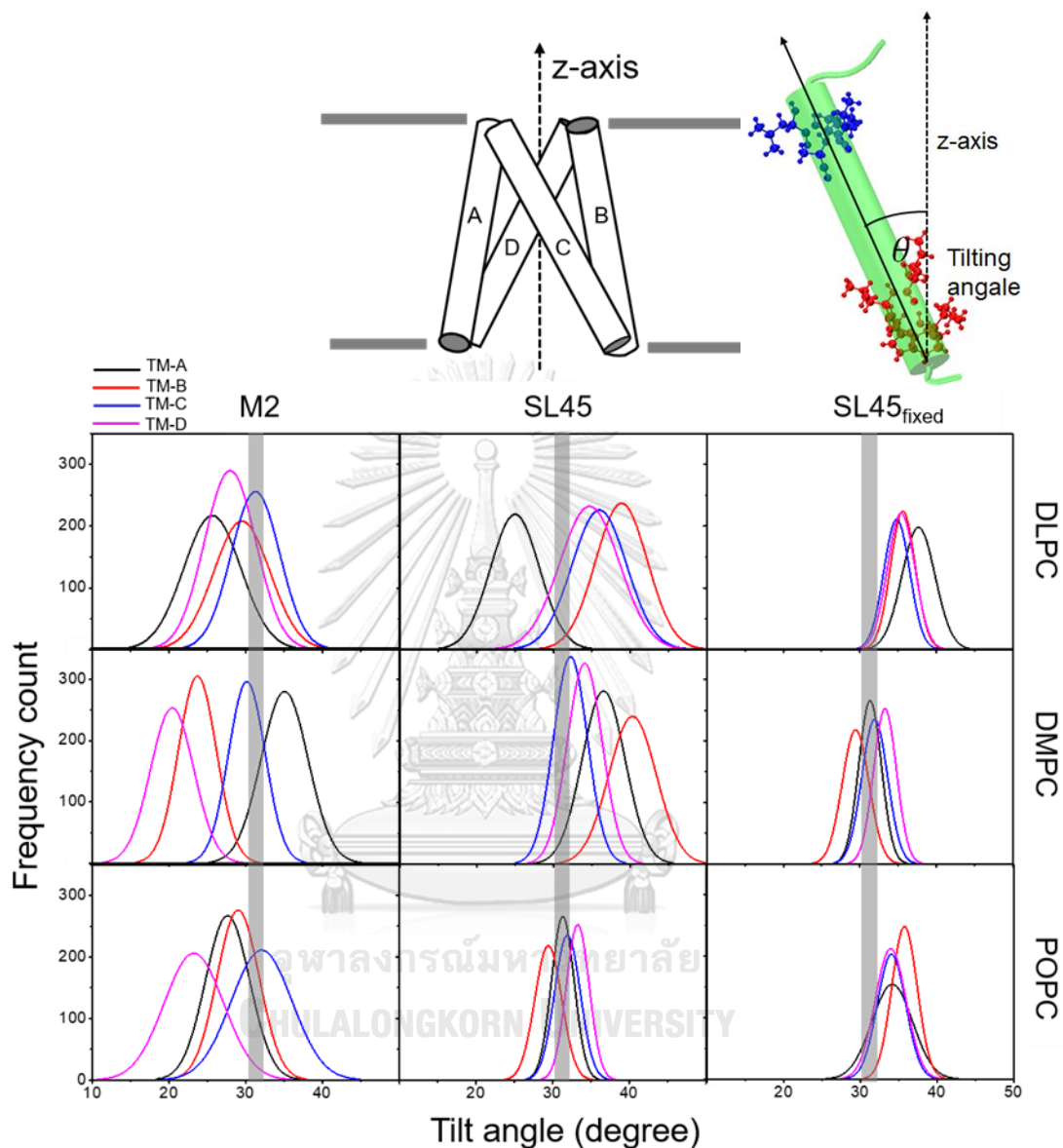


Figure 26 Cartoon representation of the four TMs rearrangement of the initial structure of the simulations.

The normal distribution of tilt angles (θ) of M2TMs calculated from the simulations of nine systems. The tilt angle of each TM is defined as the angle between the helical axis and the axis normal to the bilayer plane (the z-axis). In the initial x-ray structure, the four TMs has the fourfold symmetric arrangement with the tilt angles of 30°-32° shown in grey area.

Chapter 5

Conclusion

This research focused on an investigation of conformational perturbation of M2 channel due to changes in acyl chain length of phospholipid bilayer by using all-atomic molecular dynamics simulations. The study provided detailed insight into structural changes of M2 channel at atomic levels. The MD results were compared with experimental data obtained from spin-label EPR spectroscopy. The study showed that two major factors cause structural rearrangement in the transmembrane domain of the channel. The impact of the hydrophobic thickness of phospholipid bilayer can substantially influence the stability of TMs orientation by breaking the symmetry arrangement of the channel. The effect of the spin label attached to M2 itself can also induce conformational changes in the transmembrane domain of the channel. The structural analysis of MD data was found to be consistent with the previous studies using EPR experiments. Particularly, the MD results obtained from the DLPC and POPC lipid systems were in good agreement with the EPR spin-spin coupling data.

REFERENCES

1. Skehel, J. J.; Wiley, D. C., Receptor binding and membrane fusion in virus entry: The influenza hemagglutinin. *Annual Review of Biochemistry* **2000**, *69*, 531-569.
2. Colman, P. M., INFLUENZA-VIRUS NEURAMINIDASE - STRUCTURE, ANTIBODIES, AND INHIBITORS. *Protein Sci.* **1994**, *3*, 1687-1696.
3. Mould, J. A., et al., Mechanism for proton conduction of the M-2 ion channel of influenza A virus. *J. Biol. Chem.* **2000**, *275*, 8592-8599.
4. Mould, J. A., et al., Permeation and activation of the M-2 ion channel of influenza A virus. *J. Biol. Chem.* **2000**, *275*, 31038-31050.
5. Dong, H., et al., Proton Release from the Histidine-Tetrad in the M2 Channel of the Influenza A Virus. *J. Phys. Chem. B* **2014**, *118*, 12644-12651.
6. Pinto, L. H., et al., Influenza virus M2 protein has ion channel activity. *cell* **1992**, *69*, 517-528.
7. Liang, R. B., et al., Acid activation mechanism of the influenza A M2 proton channel. *Proc. Natl. Acad. Sci. U. S. A.* **2016**, *113*, E6955-E6964.
8. Hu, F. H., et al., Mechanisms of Proton Conduction and Gating in Influenza M2 Proton Channels from Solid-State NMR. *Science* **2010**, *330*, 505-508.
9. Chizmakov, I. V., et al., Selective proton permeability and pH regulation of the influenza virus M2 channel expressed in mouse erythroleukaemia cells. *J. Physiol.-London* **1996**, *494*, 329-336.
10. Hong, M.; DeGrado, W. F., Structural basis for proton conduction and inhibition by the influenza M2 protein. *Protein Sci.* **2012**, *21*, 1620-1633.
11. Min, J. Y.; Subbarao, K., Cellular targets for influenza drugs. *Nat. Biotechnol.* **2010**, *28*, 239-240.
12. Pinto, L. H.; Lamb, R. A., The M2 proton channels of influenza A and B viruses. *J. Biol. Chem.* **2006**, *281*, 8997-9000.
13. Horimoto, T.; Kawaoka, Y., Influenza: Lessons from past pandemics, warnings from current incidents. *Nat. Rev. Microbiol.* **2005**, *3*, 591-600.
14. Cross, T. A., et al., M2 protein from Influenza A: from multiple structures to

biophysical and functional insights. *Current Opinion in Virology* **2012**, *2*, 128-133.

15. Dong, H., et al., Exploring Histidine Conformations in the M2 Channel Lumen of the Influenza A Virus at Neutral pH via Molecular Simulations. *J. Phys. Chem. Lett.* **2013**, *4*, 3067-3071.

16. Schnell, J. R.; Chou, J. J., Structure and mechanism of the M2 proton channel of influenza A virus. *Nature* **2008**, *451*, 591-U12.

17. Duong-Ly, K. C., et al., The conformation of the pore region of the M2 proton channel depends on lipid bilayer environment. *Protein Sci.* **2005**, *14*, 856-861.

18. Saotome, K., et al., Influenza A M2 Protein Conformation Depends on Choice of Model Membrane. *Biopolymers* **2015**, *104*, 405-411.

19. Vanommeslaeghe, K.; Guvench, O., Molecular mechanics. *Current pharmaceutical design* **2014**, *20*, 3281-3292.

20. Landau, D. P.; Binder, K., *A guide to Monte Carlo simulations in statistical physics*. Cambridge university press: 2014.

21. Hospital, A., et al., Molecular dynamics simulations: advances and applications. *Advances and applications in bioinformatics and chemistry: AABC* **2015**, *8*, 37.

22. Phillips, J. C., et al., Scalable molecular dynamics with NAMD. *J. Comput. Chem.* **2005**, *26*, 1781-1802.

23. Case, D. A., et al., The Amber biomolecular simulation programs. *J. Comput. Chem.* **2005**, *26*, 1668-1688.

24. Hess, B., et al., GROMACS 4: Algorithms for highly efficient, load-balanced, and scalable molecular simulation. *J. Chem. Theory Comput.* **2008**, *4*, 435-447.

25. Allen, M. P., Introduction to molecular dynamics simulation.

26. Cramer, C. J.; Bickelhaupt, F., Essentials of computational chemistry. *ANGEWANDTE CHEMIE-INTERNATIONAL EDITION IN ENGLISH-* **2003**, *42*, 381-381.

27. Seetharaman, S., *Treatise on Process Metallurgy, Volume 1: Process Fundamentals*. Newnes: 2013; Vol. 1.

28. Zhang, J., *Molecular Dynamics Analyses of Prion Protein Structures: The Resistance to Prion Diseases Down Under*. Springer: 2018; Vol. 10.

29. Humphrey, W., et al., VMD: Visual molecular dynamics. *J. Mol. Graph.* **1996**, *14*, 33-38.

30. Huang, J.; MacKerell, A. D., CHARMM36 all-atom additive protein force field: Validation based on comparison to NMR data. *J. Comput. Chem.* **2013**, *34*, 2135-2145.
31. Seeber, M., et al., Wordom: A User-Friendly Program for the Analysis of Molecular Structures, Trajectories, and Free Energy Surfaces. *J. Comput. Chem.* **2011**, *32*, 1183-1194.
32. Sezer, D., et al., Multifrequency electron spin resonance spectra of a spin-labeled protein calculated from molecular dynamics simulations. *Journal of the American Chemical Society* **2009**, *131*, 2597-2605.
33. Vardeman, C. F., et al., The Langevin Hull: Constant Pressure and Temperature Dynamics for Nonperiodic Systems. *J. Chem. Theory Comput.* **2011**, *7*, 834-842.
34. Feller, S. E., et al., CONSTANT-PRESSURE MOLECULAR-DYNAMICS SIMULATION - THE LANGEVIN PISTON METHOD. *J. Chem. Phys.* **1995**, *103*, 4613-4621.
35. Darden, T., et al., PARTICLE MESH EWALD - AN N.LOG(N) METHOD FOR EWALD SUMS IN LARGE SYSTEMS. *J. Chem. Phys.* **1993**, *98*, 10089-10092.



จุฬาลงกรณ์มหาวิทยาลัย
CHULALONGKORN UNIVERSITY

VITA

NAME Channarong Khрутто

DATE OF BIRTH 4 Oct 1993

PLACE OF BIRTH Bangkok, Thailand

INSTITUTIONS ATTENDED 1998-2003 Primary School - Wat Nimmanoradee School
2004-2008 Secondary School - Wat Nuannoradit School
2009-2011 High School - Wat Nuannoradit School
2012-2015 Bachelor of Science (Chemistry) -
Chulalongkorn University

HOME ADDRESS 403 Petchkasem 55/2, Laksong, Bangkae, Bangkok 10160

